Supplementary Materials

Role of inner-sphere complex interaction in phosphate removal by metal-organic frameworks: experimental and theoretical investigation

Vaishali Choudhary[a], Danil W. Boukhvalov[b,c], Ligy Philip*[a],

[a]Environmental and Water Resources Engineering Division, Department of Civil Engineering, IIT Madras, Chennai 600 036, India

[b]College of Science, Nanjing Forestry University, 159 Longpan Road, Nanjing 210037, PR China

[c]Institute of Physics and Technology, Ural Federal University, Mira Str. 19, 620002 Yekaterinburg, Russia

*** Corresponding Author, E-mail: ligy@iitm.ac.in**

Text S1 Material and Method

SM 2.1. Materials

All chemicals used in the study, including aluminum chloride ($AlCl_3 \cdot 6H_2O$, 99%), ferric chloride hexahydrate ($FeCl_3 \cdot 6H_2O$, 99%), zirconyl chloride octahydrate ($ZrOCl_4.8H_2O$, 98%), 2-amino terephthalic acid (BDC-NH_2, 99 %), potassium dihydrogen phosphate (KH_2PO_4, 99%), potassium chloride (KCl, 99%), potassium sulfate (K_2SO_4, 99%), potassium bicarbonate ($KHCO_3$, 99.5 %), potassium carbonate (K_2CO_3, 99.7 %), sodium chloride (NaCl, 99%), ammonium molybdate tetrahydrate ($(NH_4)_6Mo_7O_{24} \cdot 4H_2O$, 83%), stannous chloride ($SnCl_2$), sodium hydroxide (NaOH, 99.9 %), Nafion 5 wt. %, carbon black (Vulcan XC 72R), N, N-dimethyl formamide (DMF, 99.9%), hydrochloride acid (HCl, 37 %), glycerol (99.5%), ethyl alcohol (99%) were procured from Merck Chemical (India). The chemicals were used without further purification.

SM 2.2 Synthesis and characterization of MOFs

For the synthesis of UiO-66-NH_2, 125 mg of $ZrCl_4.8H_2O$ was dissolved in 5 mL of DMF, to which 1 mL of concentrated HCl was added. The resulting mixture was ultrasonicated. Simultaneously, 134 mg of BDC-NH_2 was dissolved in 10 mL of DMF. Both the solutions (metal and organic linker) were mixed and ultrasonicated for 30 min. Later the mixture was heated to 80 °C for 12 h. The pale-yellow precipitate, obtained after the reactions, was filtered and then thoroughly washed (3 times) with DMF and ethanol. The resulting product was dried in a vacuum oven (200-500 psi) at 90 °C for 12 h [1, 2].

The NH_2-MIL-101 (Fe) was prepared similar to previously reported work [3, 4], wherein 0.225 g of BDC-NH_2 was dissolved in DMF (15 mL) and ultrasonicated for 15 min. In another beaker, 0.675 g of $FeCl_3 \cdot 6H_2O$ was dissolved in DMF (15 mL). Both the solutions were mixed slowly and kept for ultrasonication for 30 min. Finally, the solutions were heated in an oven at 110 °C for 20 h under reduced pressure. The brown precipitate was then collected by centrifugation and washed three times with DMF and ethanol. The obtained material was dried at 150 °C for 10 h under reduced pressure.

To synthesize NH_2-MIL-101(Al), 0.56 g of BDC-NH_2 and 0.51 g of $AlCl_3 \cdot 6H_2O$ were dissolved in 15 mL DMF. The two solutions were mixed and then ultrasonicated for 30 min. Later, the solution was thermally treated at 150 °C for 72 h. Finally, the precipitate (yellowish

colour) was separated by centrifugation and washed three times with DMF and ethanol. Subsequently, the synthesized material was dried at 180 °C for 72 h under reduced pressure [5].

The surface morphologies of the synthesized MOFs were studied using a scanning electron microscope (SEM) (Quanta 200 SEM (FEI, Hillsboro, Oregon)). X-ray diffraction (XRD) patterns were analyzed by D-8 Discover X-ray diffractometer (Bruker, Billerica, Massachusetts) CuKα radiation in the 2-theta range of 2–40° to examine the crystallinity. The organic functional groups were identified in attenuated total reflectance (ATR) mode using a PerkinElmer spectrophotometer (Akron, Ohio, USA) in the wavenumber range 500-4000cm^{-1}. The Brunauer-Emmett-Teller surface area, pore volume, and pore size distribution were determined using ASAP 2020-porosimeter (Micromeritics, USA). The point of zero charges was investigated using the pH drift method [6] and Horiba Particle size analyzer and zeta potential (Germany).

SM 2.3.3 Effect of environmental parameters

The effect of pH, organic matter, and co-existing anions on phosphate removal was evaluated by conducting adsorption studies. Phosphate (50 mg P/L) adsorption was examined in the pH range 2.0–12.0 with NH_2-MIL-101 (Fe), NH_2-MIL-101 (Al), and UiO-66-NH_2 dose of 1 g/L. NaOH (0.1 M) and HCl (0.1 M) were used to control the solution pH throughout the experiments. The selectivity of the adsorbent for phosphate removal was evaluated by conducting adsorption studies in the presence of co-existing anions. 10 mM of Cl^-, NO_3^-, SO_4^{2-}, HCO_3^-, and CO_3^{2-} were introduced to phosphate solution (50 mg P/L or 1.6 mM) at an adsorbent dose of 1 g/L. The system was equilibrated in a shaker (120 rpm) for 120 min at 25± 0.2 °C. To study the effect of organic matter, humic acid (10 and 50 mg/L) was added to 50 mg P/L phosphate solution with an adsorbent dose of 1 g/L.

SM 2.5 Theoretical modelling

SM 2.5.1 Kinetic modelling

Initially, pseudo-first-order (Eq. S1) and pseudo-second-order (Eq S2) kinetic models were used to describe the rate of the adsorption process [7, 8]. The experimental data were fitted to non-linear pseudo-first-order and pseudo-second-order kinetic equations, and model constants were determined using Origin 2021 software.

$$\text{Pseudo-first-order: } q_t = q_e(1 - exp(-kt)) \quad \text{(S1)}$$

Pseudo-second-order: $$q_t = \frac{K_2 q_e^2 t}{1 + K_2 q_e t}$$ (S2)

Where q_e (mg/g): the amount of phosphate adsorbed by the MOFs at equilibrium and at time t (min), k_1 (1/min), and K_2 (g/mg/min) are the rate constants for pseudo-first and second-order equations.

SM2.5.2 Equilibrium model

The experimental data were fitted into the empirical models, including Freundlich (Eq. S3) and Langmuir (Eq. S4). The model constants were calculated by non-linear analysis using Origin 21 software.

Freundlich: $$q_e = k_f C_e^{1/n}$$ (S3)

Langmuir: $$q_e = \frac{Q^o b\, C_e}{1 + bC_e}$$ (S4)

Where k_f is Freundlich adsorption constant or indicative capacity ((mg/g)/(mg/L)^n), n defines the adsorption intensity (vary between 0 and 1), Ce (mg P/L) is phosphate concentration at equilibrium, q_e (mg P/g) is the phosphate adsorbed at equilibrium, b (L/mg) is the Langmuir constant, and Q° (mg P/g) is the monolayer adsorption capacity.

Additionally, statistical physics modeling was carried out to elucidate the sorption mechanism occurring at the interface of adsorbate and adsorbate. The adsorption behavior of phosphate ions on MOFs was assessed for four conditions [9]:

i) Monolayer phosphate adsorption with uniform coverage over identical adsorption sites (MLM):

$$q = \frac{nN_m}{1 + (\frac{C_{0.5}}{C})^n}$$ (S5)

ii) Monolayer phosphate on two different active sites possessing two different energies (MLM-2):

$$q = \frac{n_1 N_{m1}}{1 + (C_1/C)^{n1}} + \frac{n_2 N_{m2}}{1 + (C_2/C)^{n2}}$$ (S6)

iii) Double layer adsorption of phosphate with the same energy of active sites (DLM):

$$q = n\,N_m \frac{(C/C_{0.5})^n + 2(C/C_{0.5})^{2n}}{1 + (C/C_{0.5})^n (C/C_{0.5})^{2n}} \quad \text{(S7)}$$

iv) Multilayer adsorption with finite layers (FLM):

$$q = n\,N_m \frac{(C/C_1)^n (1 - (N_f + 1)C/C_2)^{nN_f} + N_f (C/C_2)^{n\,(Nf+1)}}{(1 - (C/C_2)^n)(1 - (C/C_2)^n + C/C_1)^n - (C/C_1)^n (C/C_2)^{n\,(Nf)}} \quad \text{(S8)}$$

Where n represents the number of phosphate ions captured on the receptor site with the same energy, n_1 and n_1 are the phosphate ions adsorbed in monolayer and double layer, Nf is ions adsorbed at saturation, $C_{0.5,}$ C_1 and, C_2 are the half-saturation concentration of the layer formed during sorption (mg/L), and N_m is the density of functional groups or active sites on MOFs for phosphate adsorption (mg/g). All models were simulated to the equilibrium data using Origin 2021 via Levenberg -Marquardt iterating algorithm using multivariable non-linear regression tools.

Error functions, including coefficient of determination (R^2) (Eq S9), the sum of the square of error (SSE) (Eq 10), and chi-square (χ^2) (Eq S11), were used to verify the applicability of the empirical, phenomenological, and statistical model. The model correctness and parameter unbiasedness were considered when 95 % of the estimated values were within ±5 SSE of the actual value.

$$R^2 = \frac{\sum_1^n \left[q_{exp} - \bar{q_{cal}}\right]^2}{\sum_1^n \left[q_{exp} - \bar{q_{cal}}\right]^2 + \sum_1^n \left[q_{exp} - \bar{q_{cal}}\right]^2} \quad \text{(S9)}$$

$$SSE = \sum_1^n \left[q_{exp} - q_{cal}\right]^2 \quad \text{(S10)}$$

$$\chi 2 = \sum_{1}^{n} \frac{[q_{exp} - q_{cal}]^2}{q_{cal}} \quad \text{(S11)}$$

Where q_{exp} and q_{cal} (mg P/g) are the experimental and calculated value of phosphate uptake, and n is the number of observations (or data points) in the experiment.

SM 2.5.3 Density functional theory calculations

Density functional theory (DFT) calculations were performed to elucidate the interaction of phosphate ($H_2PO_4^-$) and co-existing anions with NH_2-MIL-101 (Fe), NH_2-MIL-101 (Al), and UiO-66-NH_2. The crystalline structures of NH_2- MIL-101 (Fe), NH_2-MIL-101 (Al), and UiO-66-NH_2 were reproduced from [10, 11]. The pseudopotential code SIESTA model [12] was applied for structure simulation and modeling of phosphate adsorption. All calculations were performed using the generalized gradient approximation (GGA-PBE) with spin-polarization [13] by implementing correction for weak interactions, i.e., van der Waals forces correction [14]. During the optimization, the ion cores were described by norm-conserving and non-relativistic pseudopotentials [15]. The cut of radius used for NH_2- MIL-101 (Fe), NH_2-MIL-101 (Al), and UiO66-NH_2 are summarized in Table S1. The wave functions were expanded with localized orbitals and a double-ζ plus polarization basis set for non-hydrogen species. The optimization of the atomic positions, the convergence of the force, and total energy were performed with an accuracy of 0.04 eV/Å and 1 meV, respectively. All calculations were carried out with an energy mesh cut-off of 300 Ry and a *k*-point mesh of 3×3×3 in the Monkhorst-Pack scheme [16]. For modeling, it was essential to have an accurate description of the adsorption properties of the MOFs. Since NH_2-MIL-101 and UiO-66- NH_2 systems contain more than thousands of atoms in elementary cells, using the realistic structure for the modelling is impractical. Accordingly, similar to [17], the adsorption on MOF systems was modeled by the systems which contain metal-oxide core and six linkers.

The adsorption of phosphate on NH_2-MIL-101 and UiO-66-NH_2 was considered a two-step process. In the first step, water molecules are removed from metal centers. Later, the adsorption of phosphate occurs (on the same site where water is removed) [2, 17]. The energy of the water removal from active sites can be calculated by Eq. S12

$$E_w = \frac{(E_1 + nE_{mol} - E_o)}{n} - H_{vap} \quad \text{(S12)}$$

The second step in the calculation is simultaneous water removal and phosphate adsorption on the metallic center of NH_2-MIL-101 and UiO-66-NH_2. The energy of adsorption we calculated by Eq.S13

$$E_{ads} = \frac{\left(E_1 - E_o - nE_{mol} - nH_{vap} - n - E_{ph}\right)}{n} \quad \text{(S13)}$$

where E_0 and E_1 are the energy of MOFs before and after the removal of n water molecules and adsorption of n phosphate molecules, E_{mol} is the energy of single non-interaction water molecules, E_{ph} is the energies of phosphate molecules, and H_{vap} is the experimental enthalpy of water vaporization. Since the process of water removal does not lead to the formation of new covalent bonds or phase transition, we have omitted the contribution from the entropy in the total energy of the process.

List of Tables

Table S1. Cut off radi of atom in NH_2-MIL-101 (Fe), NH_2-MIL-101 (Al), and UiO-66-NH_2

Atoms	Cut off radi (au)		
	NH_2-MIL-101 (Fe)	NH_2-MIL-101 (Al)	UiO-66- NH_2
Zr	-	-	2.52
Fe	2.12	-	-
Al	-	2.06	-
O	1.27	1.47	1.15
C	1.14	1.14	1.14
N	1.45	1.48	1.45
H	1.25	1.25	1.25

Table S2. Model constant for adsorption equilibrium data after fitting to statistical physics models.

Model	Parameters	NH_2-MIL-101 (Al)	NH_2-MIL-101 (Fe)	UiO-66-NH_2
Monolayer	N_M (mg/g)	79.28 ± 29.5	84.9 ± 25.8	90.33 ± 6.24
	n	0.81 ± 0.17	0.62 ±0.07	1.44 ±0.16
	R^2	0.983	0.993	0.993
	$\chi 2$	52.89	20.78	25.74
	SSE	264.4	128.7	103.9
Monolayer with two different energies	N_M (mg/g)	72.28 ± 0.28	88.08±0.85	86.28 ± 0.28
	n_1	1.32 ±0.15	1.77 ± 0.29	1.58 ± 0.83
	n_2	3.92 ±0.58	1.86 ± 0.13	5.21 ± 0.21
	R^2	0.996	0.994	0.997
	$\chi 2$	3.72	3.18	6.69
	SSE	0. 46 ± 0.21	0.022 ± 0.34	1.12 ± 0.84
Double layer with one energy	N_M	115.7 ± 7.24	244.26 ± 18.81	393.2 ± 15.19
	n_1	0.81 ± 0.17	1.49 ± 7.52	0.63 ± 0.58
	R^2	0.971	0.988	0.986
	$\chi 2$	66.11	32.18	25.97
	SSE	264.4	128.7	103.7
Multilayer	N_M (mg/g)	112 ± 10.41	67.08 ± 3.23	57.87 ± 4.19
	nf	0.15 ± 4.4	0.161 ± 0.81	0.216 ± 0.19
	n_2	16.8 ± 0.96	10.9 ± 0.24	12.5 ± 0.31
	n_1	0.041 ± 0.17	0.049 ± 7.52	0.063 ± 0.58
	R^2	0.771	0.688	0.586
	$\chi 2$	96.11	325.4	0158.3
	SSE	624	228.7	134.7

List of Figure

Figure S1 a) N_2 sorption and desorption curve and b) pore size distribution of NH_2-MIL-101 (Fe), NH_2-MIL-101 (Al), and UiO-66- NH_2.

Figure S2. Adsorption kinetic for phosphate adsorption onto NH_2-MIL-101 (Fe), NH_2-MIL-(Al), and UiO-66-NH_2 fitted to a) pseudo-first-order, b) pseudo-second-order kinetic model.

Figure S3. FT-IR spectra of regenerated NH_2-MIL-101 (Fe), NH_2-MIL-101 (Al), and UiO-66- NH_2 using (a) NaOH (0.01M), (b) NaCl (1% w/v), (c) Na_2CO_3 (0.01 M) as eluent.

Figure S4. PXRD spectra of MOFs regenerated using 0.01 M NaOH.

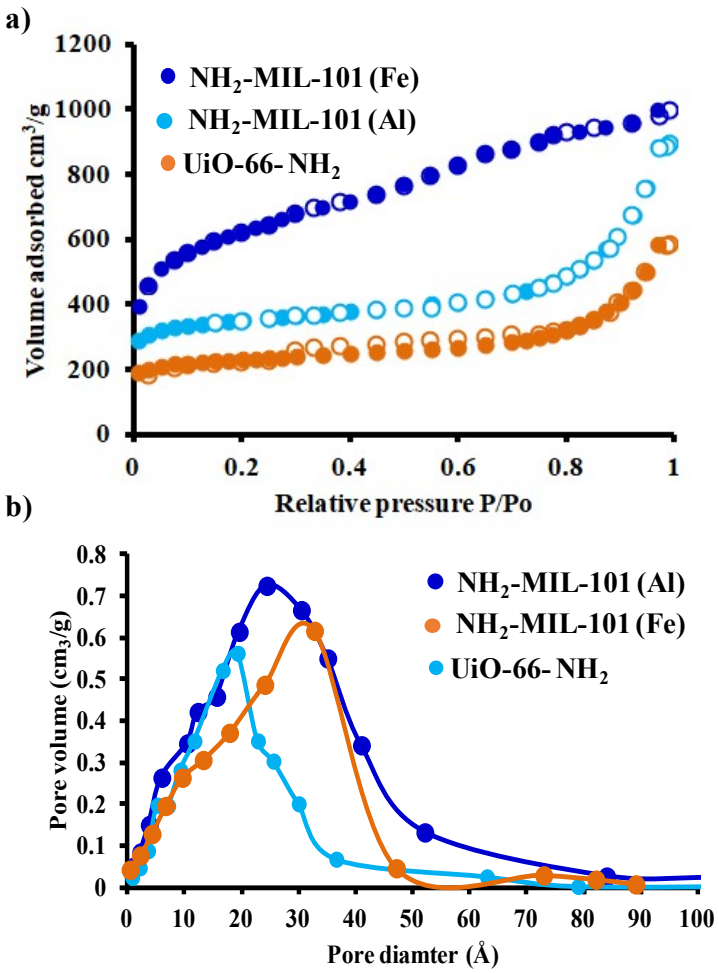

Figure S1 a) N_2 sorption and desorption curve where dark circle (●) represent adsorption and empty circle (o) represents desorption, b) pore size distribution of NH_2-MIL-101 (Fe), NH_2-MIL-101 (Al), and UiO-66- NH_2.

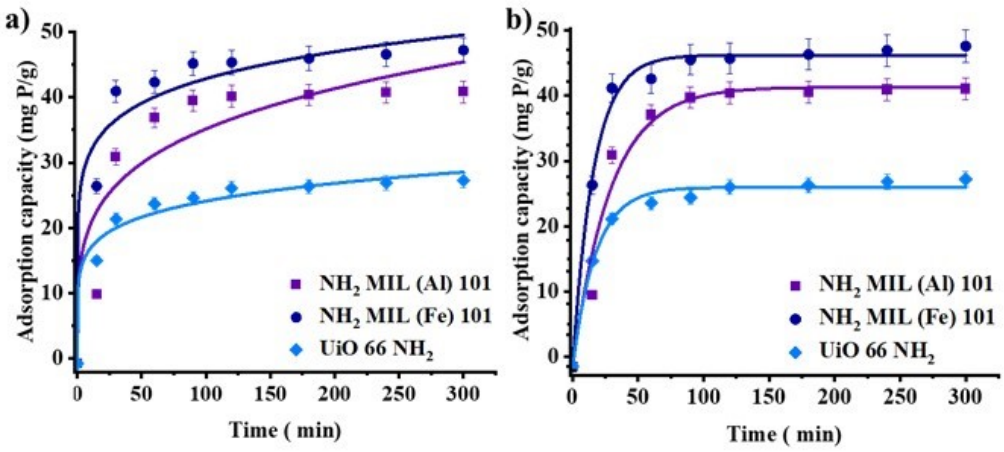

Figure S2. Phosphate adsorption kinetic onto NH_2-MIL-101 (Fe), NH_2-MIL-101 (Al), and UiO-66-NH_2 fitted to (a) pseudo-first-order, (b) pseudo-second-order kinetic model.

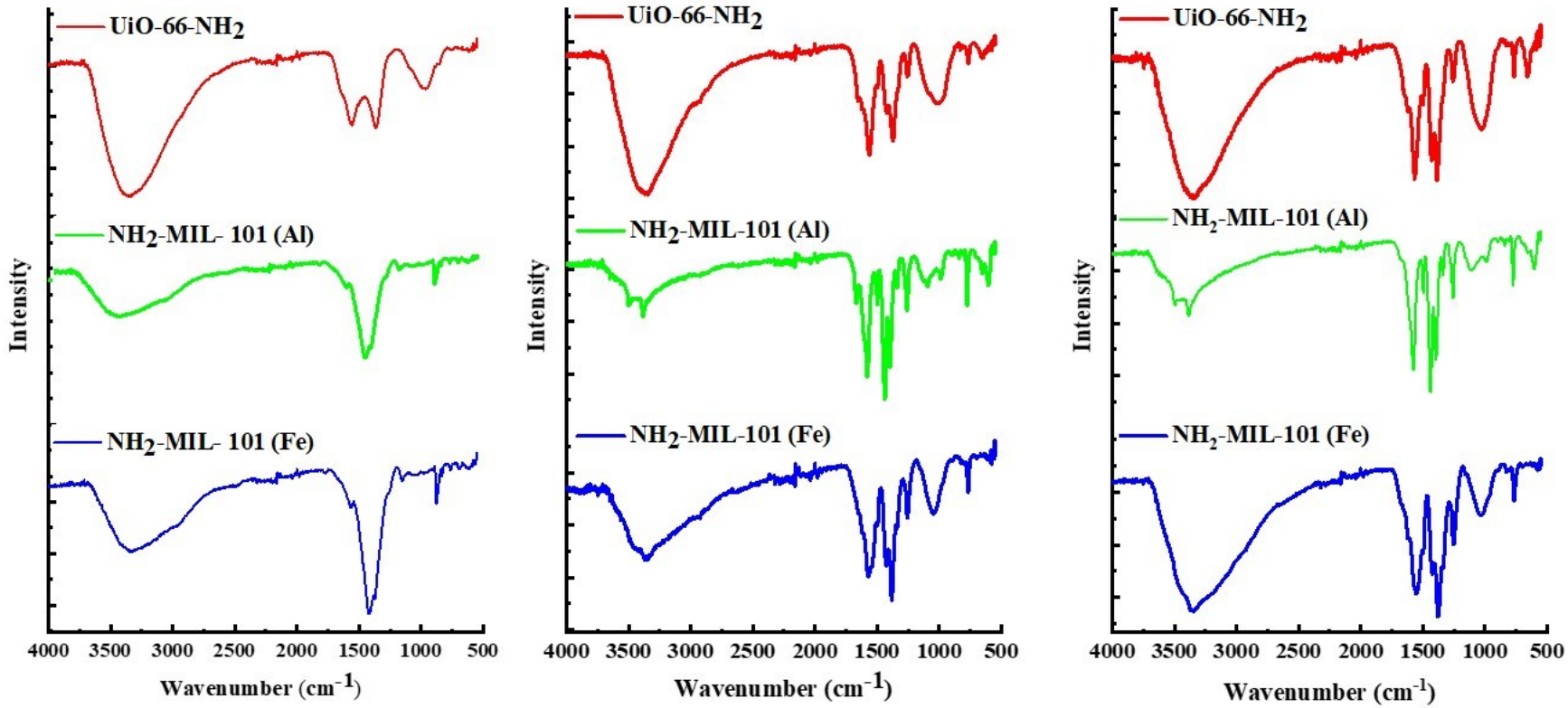

Figure S3. FT-IR spectra of regenerated NH_2-MIL-101 (Fe), NH_2-MIL-101 (Al), and UiO-66- NH_2 using (a) NaOH (0.01M), (b) NaCl (1% w/v), (c) Na_2CO_3 (0.01 M) as eluent.

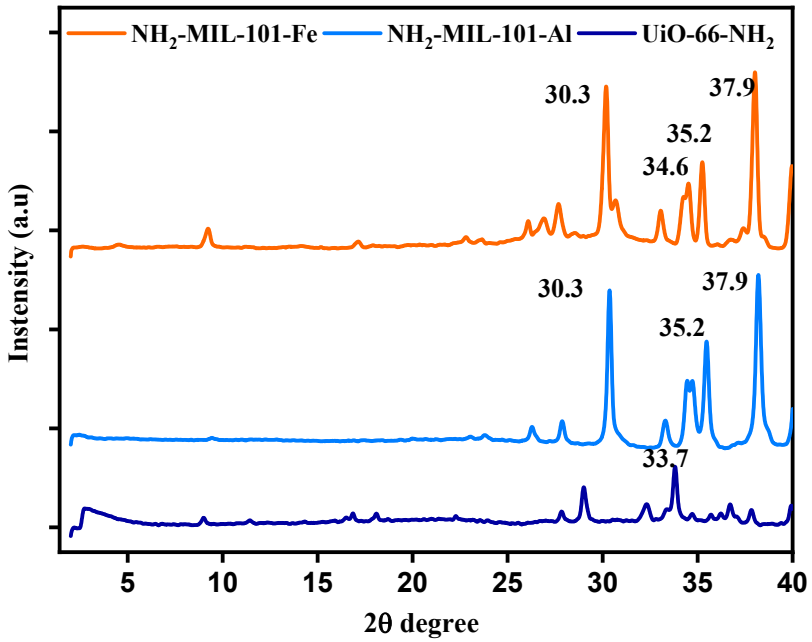

Figure S4. PXRD spectra of regenerated in 0.01 M NaOH.

References

1. M. J. Katz, Z. J. Brown, Y. J. Colón, P. W. Siu, K. A. Scheidt, R. Q. Snurr, J. T. Hupp and O. K. Farha, A facile synthesis of UiO-66, UiO-67 and their derivatives, *Chemical Communications*, 2013, **49**, 9449-9451.
2. K. Vellingiri, A. Deep, K.-H. Kim, D. W. Boukhvalov, P. Kumar and Q. Yao, The sensitive detection of formaldehyde in aqueous media using zirconium-based metal organic frameworks, *Sensors and Actuators B: Chemical*, 2017, **241**, 938-948.
3. R. Liu, L. Chi, X. Wang, Y. Wang, Y. Sui, T. Xie and H. Arandiyan, Effective and selective adsorption of phosphate from aqueous solution via trivalent-metals-based amino-MIL-101 MOFs, *Chem. Eng.J*, 2019, **357**, 159-168.
4. N. V. Maksimchuk, K. A. Kovalenko, V. P. Fedin and O. A. Kholdeeva, Cyclohexane selective oxidation over metal–organic frameworks of MIL-101 family: superior catalytic activity and selectivity, *Chemical Communications*, 2012, **48**, 6812-6814.
5. P. Serra-Crespo, E. V. Ramos-Fernandez, J. Gascon and F. Kapteijn, Synthesis and characterization of an amino functionalized MIL-101 (Al): separation and catalytic properties, *Chemistry of Materials*, 2011, **23**, 2565-2572.
6. Y. Yang, Y. Chun, G. Sheng and M. Huang, pH-dependence of pesticide adsorption by wheat-residue-derived black carbon, *Langmuir*, 2004, **20**, 6736-6741.
7. Y.-S. Ho and G. McKay, Pseudo-second order model for sorption processes, *Process biochemistry*, 1999, **34**, 451-465.
8. S. K. Lagergren, About the theory of so-called adsorption of soluble substances, *Sven. Vetenskapsakad. Handingarl*, 1898, **24**, 1-39.
9. L. Sellaoui, H. Guedidi, S. Knani, L. Reinert, L. Duclaux and A. B. Lamine, Application of statistical physics formalism to the modeling of adsorption isotherms of ibuprofen on activated carbon, *Fluid phase equilibria*, 2015, **387**, 103-110.
10. O. Lebedev, F. Millange, C. Serre, G. Van Tendeloo and G. Férey, First direct imaging of giant pores of the metal− organic framework MIL-101, *Chemistry of materials*, 2005, **17**, 6525-6527.
11. L. Valenzano, B. Civalleri, S. Chavan, S. Bordiga, M. H. Nilsen, S. Jakobsen, K. P. Lillerud and C. Lamberti, Disclosing the complex structure of UiO-66 metal organic framework: a synergic combination of experiment and theory, *Chemistry of Materials*, 2011, **23**, 1700-1718.
12. J. M. Soler, E. Artacho, J. D. Gale, A. García, J. Junquera, P. Ordejón and D. Sánchez-Portal, The SIESTA method for ab initio order-N materials simulation, *Journal of Physics: Condensed Matter*, 2002, **14**, 2745.
13. J. P. Perdew, K. Burke and M. Ernzerhof, Generalized gradient approximation made simple, *Physical review letters*, 1996, **77**, 3865.
14. M. Dion, H. Rydberg, E. Schröder, D. C. Langreth and B. I. Lundqvist, Van der Waals density functional for general geometries, *Physical review letters*, 2004, **92**, 246401.
15. N. Troullier and J. L. Martins, Efficient pseudopotentials for plane-wave calculations, *Phys. Rev. B*, 1991, **43**, 1993.
16. H. J. Monkhorst and J. D. Pack, Special points for Brillouin-zone integrations, *Phys. Rev. B*, 1976, **13**, 5188.
17. K. Vellingiri, D. W. Boukhvalov, K.-H. Kim and L. Philip, Validation of 'lock-and-key'mechanism of a metal–organic framework in selective sensing of triethylamine, *RSC Adv.*, 2019, **9**, 7818-7825.